ADVANCES IN ATMOSPHERIC SCIENCES, VOL. 21, NO. 6, 2004, 909–922

# A Mesoscale Analysis of Heavy Rain Caused by Frontal and Topographical Heterogeneities on Taiwan Island

JING Li*[1] (景 丽), LU Hancheng[1] (陆汉城), WANG Hanjie[2] (王汉杰),
ZHU Min[1] (朱 民), and KOU Zheng[1] (寇 正)

[1] *Institute of Meteorology, PLA University of Science and Technology, Nanjing* 211101

[2] *Key Laboratory of Regional Climate-Environment Research for Temperate East Asia, Chinese Academy of Science, P. O. Box* 2861 (7), *Beijing* 100085

(Received 15 November 2003; revised 29 January 2004)

**ABSTRACT**

The prevailing mesoscale model MM5 (V3) is used to simulate a heavy rain case caused by interaction between a move-in front and topographical heterogeneities on Taiwan Island. It is found that both thermodynamic and dynamic fields along the front are heterogeneous in time and space. The heterogeneity becomes more significant as the effect of topography is added on. The heterogeneous distribution of physical variables along the front is the main reason for the heterogeneous frontal rain band; the optimum cooperation of the low level and upper level jet is another reason for the development of the rain band. Topography can strengthen the rainfall and causes extremely heavy rain cells. Updraft induced by topography extends to a rather low level, while the uplifted air by frontal circulation can reach to higher levels. The quasi-steady topographic circulation overlaps the frontal circulation when the front moves over Taiwan Island; the advantageous cooperation of various mesoscale conditions causes the large upward velocity on the windward side of the island.

**Key words:** frontal heterogeneity, heavy storm, topographical circulation, MM5, Taiwan Island

## 1. Introduction

Located off the southeast coast of China, Taiwan Island is climatologically within the subtropical zone. Topographically, two thirds of the island are mountains, of which five are in the south-north direction, parallel from east to west; the mountains are sequentially called Taitung Mountain, Chungyang Mountain, Hsueh Shan Mountain, Hsueh Shan Mountain, and Ali Mountain. The highest peak of Hsueh Shan Mountain is 3997 m above sea level; it is the highest peak not only on Taiwan Island, but also in southeast China. In general, the eastern island is steep with a very narrow plain area; to the western part of the island, however, the topography is rather flat and there are broad plains there. The particular topography plays a vital role in regulating the weather of Taiwan Island. Climate analysis shows that both the frequency and intensity of heavy storms (daily rainfall exceeding 50 mm) are greatest on Taiwan Island compared to the rest of China. Heavy storms not only affect various social activities, but also cause frequent flood disasters because Taiwan Island is a mountainous island. (Climatology Data Office of Fujian Province, 1987)

For some reasons, there have been few studies on heavy storms in Taiwan Island performed by the the continental meteorological researchers so far. On the other hand, there are more than 30 routine weather stations in Taiwan Island, intensive observation campaigns are possible whenever is necessary, so the heavy rain studies are very popular on Taiwan Island (Chen and Li, 1995; Chen et al., 1997). In order to understand the formation mechanism and to improve forecast accuracy of heavy storms that cause flood disasters in Taiwan Island, a mesoscale field campaign was conducted from 10 May to 27 June 1987. The campaign, known as TAMEX, aimed to detect the pre-summer weather in Taiwan Island (Chen et al., 1994; Li et al., 1997). The intense observations include air-borne measurements and radar scanning data that are not available in routine meteorological observations. Based on these datasets, some valuable results

*E-mail: jingli41@eyou.com

about the formation and development mechanism of heavy storms in Taiwan Island were obtained. Some studies have shown that the rain season of Taiwan Island is from the second ten-day period of May to the end of June and that the maximum rainfall occurs on the windward slope in the southwest monsoon region, which introduces the following heavy rain case to our study field.

There have been many studies that reveal the interaction mechanism among topography, frontogenesis and heavy rain formation (Lu and Zhao, 1997; Hao et al., 2001; Sun et al., 2002; Lou et al., 2003; Yue et al., 2003). These studies found the following common interaction mechanism: in the out-flow area in the northeast section of the south Asia cyclone, divergence occurs because of the imbalance of the wind-pressure field. On the lee side of the Tibetan Plateau, the high level trough deepens and moves to the east coast of China, the front forms in upper levels due to the horizontal shearing along the trough; as the trough approaches, the baroclinic force between the high level and low level forms, and accompanying the topographic lifting, a heavy storm occurs in the warm and wet tongue in the low level. In addition, the low level jet (LLJ) helps to transfer warm and wet air, which benefits the formation and development of the large-scale precipitation.

Referring to the special topography of Taiwan Island, Chen and Cheng (2000) studied the characteristics of the rainfall distribution and surface wind field during the 1996 and 1997 Meiyu season, and Lin et al. (2000) studied a shallow front as it passed across Taiwan Island. Hao et al. (2001) found that Taiwan Island's topography is very important in inducing the boundary layer jet and in rainfall distribution over Taiwan Island during the Meiyu season. Yeh and Chen (1998) pointed out that topography plays a dominant role in the occurrence and distribution of precipitation in the pre-summer rain season in Taiwan Island, while Cui et al. (2002) argued that the topography is important to the heavy rain but not the dominant factor: the most important factor is the abundant warm and wet air blocked in the upstream of the windward side. Nevertheless, these studies help us to understand the occurrence and development mechanism of Taiwan Island's heavy storms from different aspects.

From the numerical experimental point of view, Song and Chen (2001) simulated the formation and evolution of a mesoscale convective system (MCS) in Taiwan Island by mesoscale model MM4, studying the heavy rain case of 15–16 may 1987. The case was in the TAMEX period; they detected the process of water vapor and latent heat that affects the LLJ. Lai (2002) studied the heavy storm case from 6–8 June 1987 in the TAMEX period by mesoscale model MM5; he found that as the front moved across Taiwan Island, the topographical resistance effect caused precipitation enhancement on the windward slope, and the latent heat release and water vapor flux from the sea surface were two important factors in causing convection in the frontal zone.

We notice that the horizontal resolution of the mentioned simulation study was 60 km (Song and Chen, 2001); this is too coarse to reveal the mesoscale circulations caused by the topographical effect and the mechanism that forms and enhances the heavy storms in Taiwan Island. In the present study, a two-fold nested model of MM5 (V3) is used with a fine grid of 15 km and a coarse grid of 45 km, with which the high resolution data suitable for mesoscale analysis are obtained; this data is then used to analyze the southeastward-moving front system originating from Mainland China and its interaction process with the topographical circulation on Taiwan Island.

## 2. The numerical simulation scheme and case selection

A heavy storm occurred from 13 to 16 June 2001 in Taiwan Island. Based on the weather bulletin announced by the Taiwan Meteorological Bureau, the maximum daily rainfall on 13 June was 46.6 mm in Taiwan Island. On 14 June, a heavy rain center of 223 mm was located over Ali Mountain and one of 100.5 mm in Chiayi. The stations at which daily rainfall exceeded 50 mm include Danshui, Anpu, Tainan, Tawu, Wuchi and Jihyueh Tan; the other stations all reported more or less precipitation. On 15 June, the maximum daily rainfall was 126 mm in Hengchun; precipitation in other places was less than on 14 June. On 16 June, there was no report of heavy rain. The storm was therefore over. During the heavy storm period, a front appeared in Mainland China and moved eastward sequentially through the southeast coast of China, Taiwan Strait, and Taiwan Island, finally entering into the west Pacific Ocean. On 13 June, the front system reached southeast China, occupying a frontal line from Hangzhou, Northwest Fuzhou and Guangzhou, and afterward, the front moved continuously southeastward. At 0000 UTC 14 June, the center of the frontal cyclone was at 32.5°N, 131.5°E. At 0000 UTC 15 June, the front left Taiwan Island and the heavy rain was finished at all stations except Hengchun. So it is evident that the heavy storm was caused by the front system. The satellite cloud image shows that there was an intense cloud cluster on the windward slope in Taiwan Island as the front moved in, telling us that the topography played more or less an important role in the formation of the heavy storm.

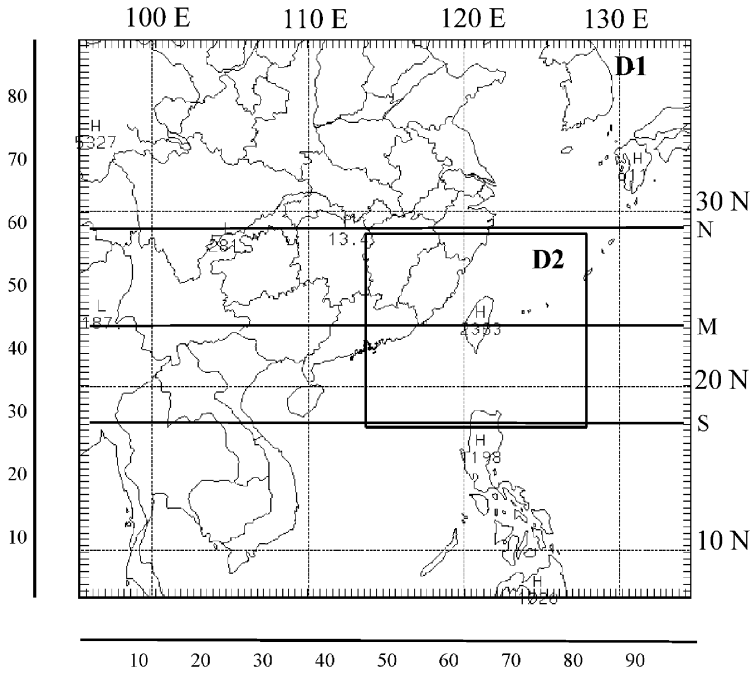


**Fig. 1.** The two-fold nested model domains.

**Table 1.** The parameterization schemes used in the study.

| Items | Outer domain | Inner domain |
|---|---|---|
| Center location | 24.0°N, 115.0°E | 24.0°N, 121.5°E |
| Grid distance | 45 km | 15 km |
| Vertical levels | 23 | 23 |
| Topography resolution | 10′ | 5′ |
| Cumulus parameterization scheme | Betts-Miller | Grell |
| Physical process | Process | Process |
| Surface parameterization scheme | High-resolution MRF scheme | High-resolution MRF scheme |
| Lateral boundary condition | Time-varied boundary | Time-varied boundary |
| Atmosphere radiation scheme | CCM2 | CCM2 |

The model simulation domain is shown in Fig. 1. The outside domain covers an area of 88×98 coarse grid points of 45-km spacing and the inner nested domain covers an area of 98×100 fine grid points of 15-km spacing. The parameters used and the selected parameterization schemes are listed in Table 1. The model outputs from the coarse model were used to analyze the synoptic-scale front formation, development, movement, and features, while those from the fine model were used to analyze the frontal mesoscale characteristics and topographical functions of Taiwan Island. The model was run with the initial and lateral boundary conditions provided by the outputs of the National Meteorological Center of China, GCM T106. The background data is from 1200 UTC 13 June to 0000 UTC 15 June with a time interval of 12 hours. The model was run over this same 36-hour period, which just covers the whole heavy rain process when the frontal system moved across Taiwan Island. The integration time step is 90 s for the coarse grid and 30 s for the fine grid.

## 3. Comparison between the observations and simulations

### 3.1 *Pressure and streamline field*

Figures 2a′ and 2b′ show the geopotential heights and streamlines at 500 hPa at 1200 UTC 14 June,

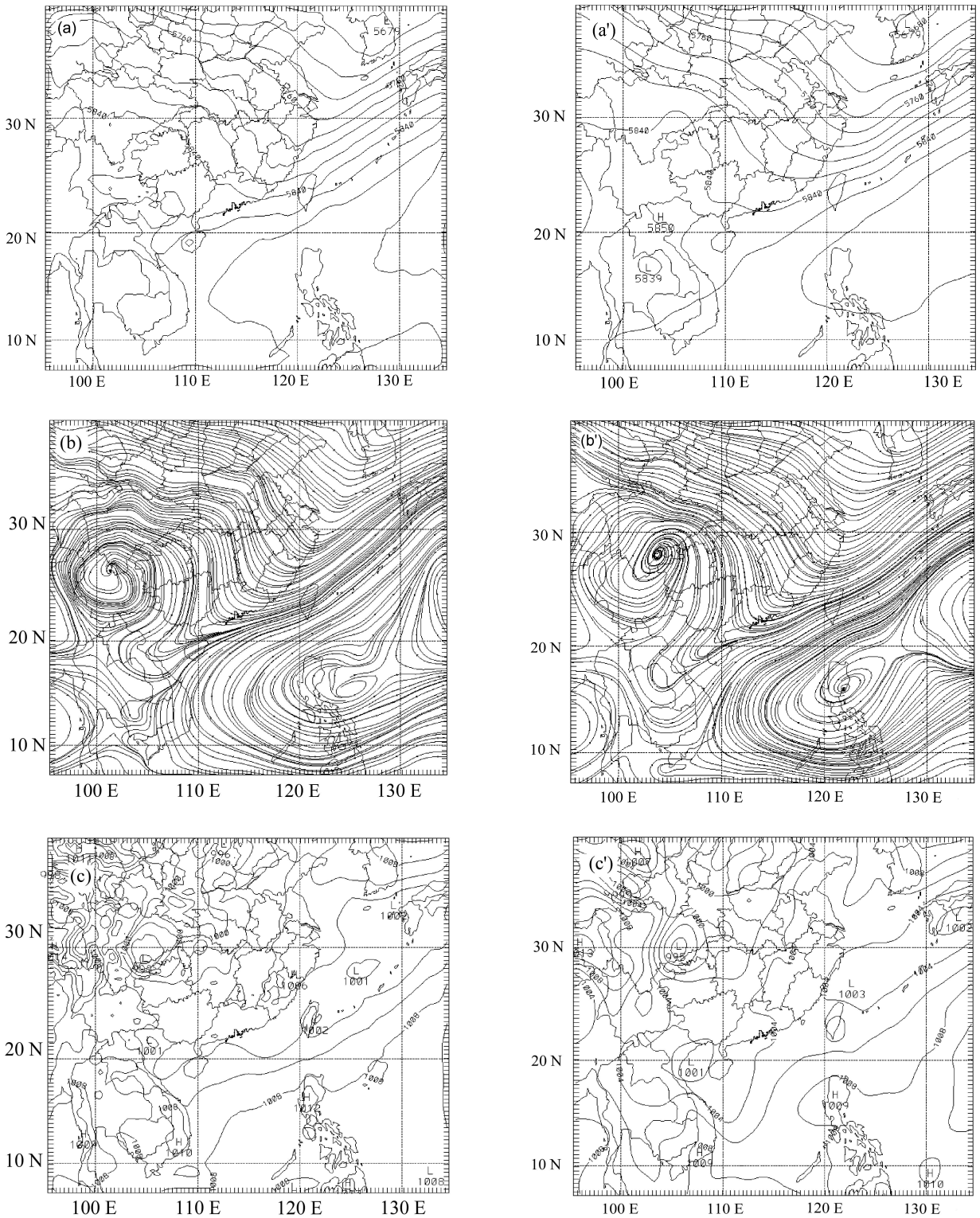


**Fig. 2.** Comparison between simulations after 24 h of integration and the analyzed observations. (a) and (b) are simulated geopotential heights (units: $m^{-2}\ s^{-2}$) and streamline at 500 hPa, and (c) is the sea level pressure (units: hPa) (a′), (b′), (c′) are the corresponding analyzed observations.

which is 24 hours after the model started. There is a strong trough in the northeast-southwest orientation in the east coast area of China; its movement and intensity are closely related to the frontal system. Compared with the figures at the initial time (omitted), the curvature of the isobaric lines in the trough area gradually turned flat, and the trough weakened accordingly (Figs. 2a′ and 2b′). The 24-h simulation (Figs. 2a and 2b) shows similar results with the observations. The 36-hour integration gives a trough position off Taiwan Island, which coincides with the observations (figures omitted). The movement of the front and frontal cyclone can be traced by the temporal variation of geopotential heights and streamline field. The simulation is in good agreement with observations. The model not only simulates the eastward movement of the trough at 500 hPa but also its weakening process. The streamline pattern and its evolutions at 500 hPa are also simulated. The cyclonic circulation in the East Coast trough area and the anticyclonic circulation related to the West Pacific subtropical high underwent an intensifying and a weakening process, which caused the movement of the low level front system.

Figure 2c shows the sea level pressure after 24 hours; the front is close to Taiwan Island, this simulated position is in good agreement with observation (Fig. 2c′), and the simulated pressure low in northeast Taiwan Island is 1001 hPa and is lower than the observed value of 1003 hPa. The pressure oscillates in the areas adjacent to Taiwan Island. Because of the coarse resolution of the observation data, they cannot reveal the mesoscale information and the pressure oscillations. It is reasonable that the quasi-permanent southwest current forms a high-pressure ridge on the windward slope and a trough on the lee side. This demonstrates the model's capability in simulating the topographical functions. The front is no longer over Taiwan Island after 36 hours of integration, which coincides with the observations. Other patterns agree with the observations as well.

The above analysis shows that a heavy storm occurring over Taiwan Island can be classified as a low level front moving on under the high level introduction of a southeastward-moving trough. This means the coarse circulation simulation is not enough: the reasonability of the precipitation simulation needs to be analyzed as well.

### 3.2 *Precipitation distribution pattern comparison*

As the front moved over the Pacific Ocean, there was no observed rainfall data over the ocean. In order to compare the simulated rainfall with observations, the simulated water vapor content was inversed to the cloud image, which was then used to compare with the satellite-observed cloud image and ascertain the reality of the simulated precipitation (Fig. 3). As compared with the actual position of the rain belt at different times, the simulated movement of the frontal rain belt is 3–6 hours later than the actual one; the model also reports some virtual rainfall over the ocean (Fig. 3a). The time delay may be caused by the fact that the satellite senses cloud immediately as it forms while the model-predicted value is the rainfall several hours later after the convective cloud forms. Another reason is that the initial condition of the model is a large-scale variable field; it takes time to trigger the intense rainfall cells. Song and Chen (2001) also obtained similar results using MM4 and MM5 for precipitation simulation. This model-introduced error should be considered when analyzing the model outputs. In this paper, the model outputs of precipitation after 12 hours of integration are used for further analysis in order to remove the virtual rain belt delay. In general, the model provides synoptic frontal precipitation as output.

By tracing the movement of the rain belt we find that at 0000 UTC 14 June 2001, the observed rain belt reached Taiwan Island. Because the simulated frontal movement was slower, the simulated rain belt was in the Strait, the cloud covered the north part of Taiwan Island, at 1200 UTC 14 June (Fig. 3) the simulated rain belt covered the west part of Taiwan Island, and at 1800 UTC 14 June the observed rain belt moved eastward continuously, so one third of eastern Taiwan Island was covered with cloud, while the simulated rain belt covered the whole of Taiwan Island.

## 4. Mesoscale structure of the frontal system

As the model simulates both large-scale circulation and precipitation distribution, the high-resolution outputs from the model are valuable for further analysis.

Figure 1 shows that Taiwan Island is close to the 62th latitudinal and 45th longitudinal grid point in the coarse grid system. Latitudinal sections are drawn at the 30th, 45th and 60th grid point in the longitudinal direction. The section at the 45th grid point crosses the Strait and Taiwan Island. The other two pass south and north of Taiwan Island respectively; the distance between these two sections is about 700 km. The physical variables at these three sections illustrate the differences in frontal structure from north to south. At 0600 UTC 14 June, the front is located over the Taiwan Strait and at 1800 UTC 14 June, it reaches Taiwan Island. By analyzing variables within the frontal system at specific times, one can understand the variable distributional pattern and its variations as the front approaches and moves across Taiwan Island. It is clear that there is a complicated interac-

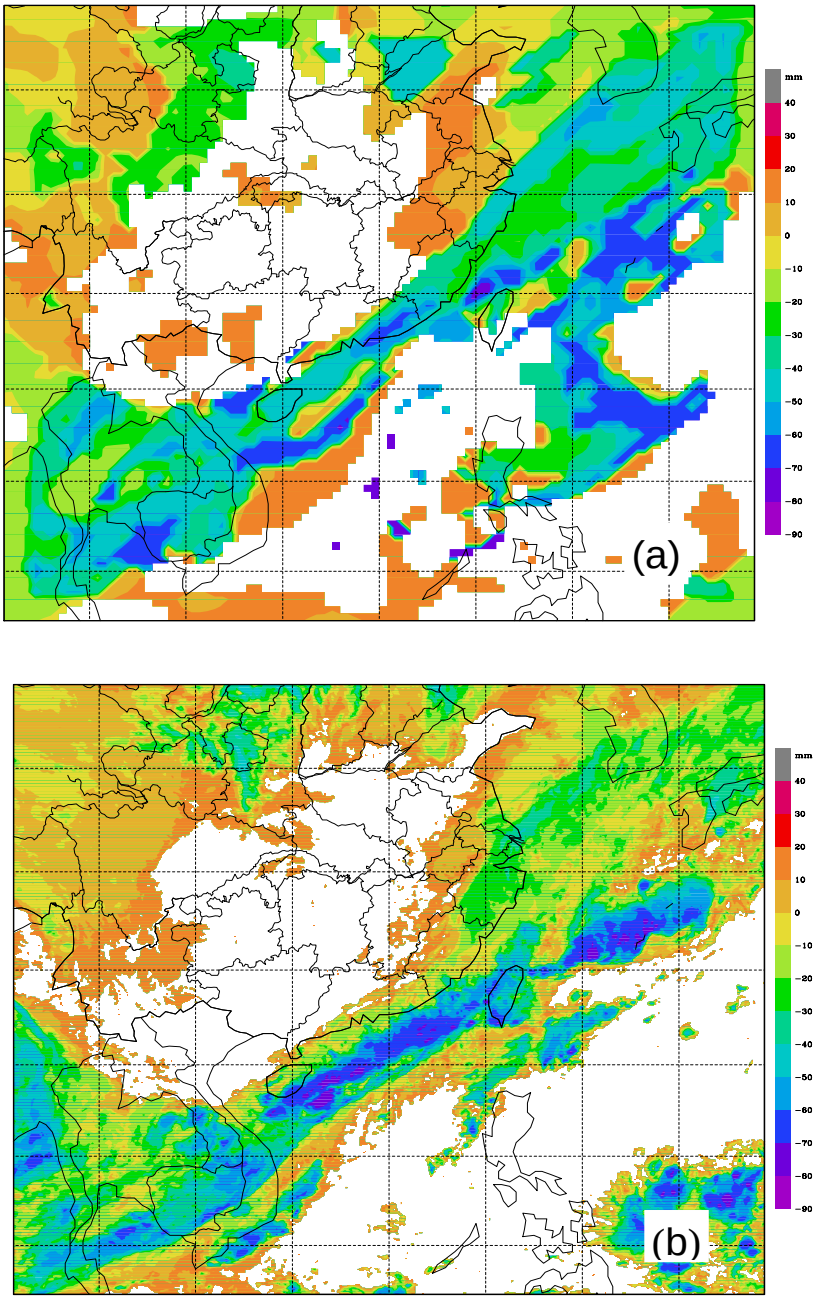


**Fig. 3.** Cloud image inversed from water vapor content of the model outputs after 24 h of integration (a) and satellite-observed cloud image (b).

tion process between the frontal system and local topography.

### 4.1 *Temperature gradient distribution in the frontal system*

The front is formed as cold and warm air masses meet. So the temperature difference directly reflects the frontal intensity. We define the temperature gradient $\Delta T$ as:

$$\Delta T = \sqrt{\left(\frac{\partial T}{\partial x}\right)^2 + \left(\frac{\partial T}{\partial y}\right)^2}$$

which is in units of K $(10\ \mathrm{km})^{-1}$. The central difference scheme is used in the corresponding gradient calculations.

**Table 2.** Locations of the maximum temperature gradient centers and the high temperature gradient belt on the 850 hPa level [units: K (10 km)$^{-1}$].

| Time June 2001 | Centers and central values of $\Delta T$ | Location of high temperature gradient zone |
|---|---|---|
| 0000 UTC 14 June | North center 0.6 K (10 km)$^{-1}$; Other area, about 0.4 K (10 km)$^{-1}$ Taiwan Island, 0.8 K (10 km)$^{-1}$ | Southeast coast of China |
| 0600 UTC 14 June | North center, 0.7 K (10 km)$^{-1}$; other area, 0.5 K (10 km)$^{-1}$; Taiwan Island, 0.8 K (10 km)$^{-1}$ | Moved southeastward to east Taiwan Strait |
| 1200 UTC 14 June | North center, >0.7 K (10 km)$^{-1}$; Taiwan Island, >0.8 K (10 km)$^{-1}$ | Move southeastward to near Taiwan Island |
| 1800 UTC 14 June | North center, 0.5 K (10 km)$^{-1}$; Taiwan Island, 0.5 K (10 km)$^{-1}$ | Reached Taiwan Island |
| 0000 UTC 15 June | North center, 0.4 K (10 km)$^{-1}$ | Moved away from Taiwan Island into west Pacific ocean |

4.1.1 *Temperature gradient at* 850 hPa

By analyzing the isotherms at 850 hPa, we find that the maximum value of the temperature gradient belt lies in the northeast-southwest direction, which is the same position as the trough of the geopotential heights. This shows the place of interaction between the cold and warm air masses that form the front.

The evolution of the temperature gradient (Table 2) shows that the front coincides with the maximum values of $\Delta T$ that shape the belt. There are several extreme centers within the belt, which illustrates that the temperature gradient within the frontal region is heterogeneous. The extreme value centers of temperature gradient show a large difference of temperature and frontal intensity. The front is then generated in this area according to frontogenesis theory. On the windward slope of Taiwan Island, there is a permanent large value center of the temperature gradient; its intensity varies with time. Close to the front, the temperature gradient is folded by the effect of topography effect and forms extreme large value centers and thus enhances the frontal circulation.

4.1.2 *The temperature gradient distribution on latitudinal sections*

Vertical cross sections are drawn at the 30th, 45th and 60th grid points from south to north along the front; these are hereafter referred to as the south (S), middle (M) and north (N) sections, respectively. (Fig. 1).

The latitudinal variation of the vertical section of temperature gradient reveals that the movable front system extends vertically to the lower part of the troposphere, while the temperature difference caused by topography affects the temperature distribution to rather higher levels. From 0000 UTC 14 June (12 hours integration) to 0600 UTC (18 hours integration), the largest value of temperature gradient appears at 920 hPa, from the 20th to the 28th grid point of the south section, which corresponds to the maximum center at 1000 hPa on the continent and relates to the frontal generation. At 0600 UTC, there is a large value center of 0.3 K (100 km)$^{-1}$ at 100 hPa. On the middle section, the large value center of the temperature gradient is at the 52nd grid point; this corresponds to Fujian province on the continent. The center remains constant. To the east of this center at the 55th grid point, there is a second large value center; its largest temperature gradient appears on the upper level of 850 hPa at 0000 UTC with a value of 0.8 K (10 km)$^{-1}$. At 0600 UTC 14 June, the quasi-constant temperature gradient center located in Fujian starts to weaken and the center to its east moves eastward; the value is 0.5 K (10 km)$^{-1}$ at 1000 hPa and 0.3 K (10 km)$^{-1}$ at 920 hPa. The temperature gradient in the upper level in western Taiwan Island does not vary so much; the average value is about 0.6 K (10 km)$^{-1}$. To the north section, the large value center of temperature gradient leans toward a cold area with height, as does the frontal surface itself. The largest value center of temperature gradient in middle-low levels of the north section moves eastward with time, and at 0600 UTC it is 0.6 K (10 km)$^{-1}$. The value at 400 hPa is 0.8 K (10 km)$^{-1}$, which tells of a high-level intensification process.

At 1200 UTC 14 June, the large value center of temperature gradient on the south section moves to Taiwan Island with the front (Fig. 4a), its near-surface intensity is about 0.8 K (10 km)$^{-1}$ extending vertically to about the 220 hPa level (Fig. 4b). On the north section, the maximum center of temperature gradient is enhanced to 0.8 K (10 km)$^{-1}$ in middle-low levels but weakens in the upper levels; its value is 0.6 K (10 km)$^{-1}$ on the 400 hPa level only.

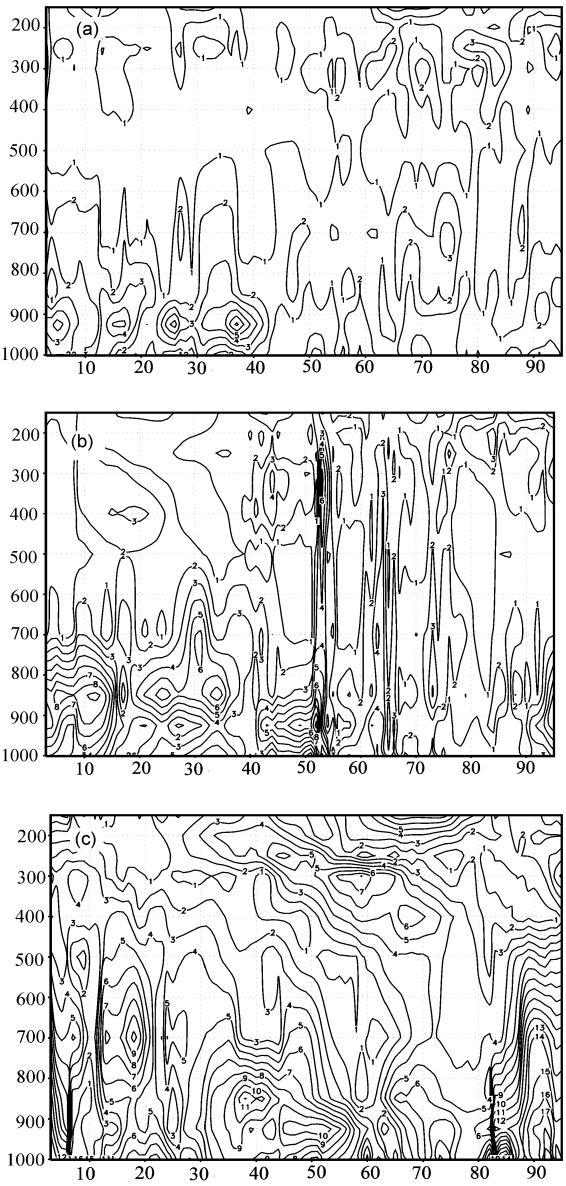


**Fig. 4.** Temperature gradient distributional features on the latitudinal sections after 24-h of integration $X$-ordinate: grid number; $Y$-ordinate hPa; a, b, c refers to south, middle and north sections respectively [units: K $(10\ \mathrm{km})^{-1}$].

The large value center on the south section moves eastward later on; its value of 0.3 K $(10\ \mathrm{km})^{-1}$ at 1800 UTC 14 June reduces to 0.2 K $(10\ \mathrm{km})^{-1}$ at 0000 UTC 15 June. The large value center on the middle section extends to an even higher level exceeding 200 hPa because of the front's approaching. At 0000 UTC 15 June, the temperature gradient on the windward slope of Taiwan Island increases in the low level as the front passes by Taiwan Island. The cold air behind the front is resisted by the windward slope and the air temperature on the lee side does not change very much, so the temperature difference before and after the mountain ridge is large. At 1800 UTC 14 June, the temperature gradient reaches 0.9 K $(10\ \mathrm{km})^{-1}$ on the north section and reaches the height of 300 hPa. At 0000 UTC 15 June the temperature gradient remains strong, the value is 1.4 K $(10\ \mathrm{km})^{-1}$ in the low level and 0.9 K $(10\ \mathrm{km})^{-1}$ in the upper level.

Based on the above analysis, we find that both the intensity and distribution patterns of temperature gradient maxima show variations along the frontal system at same moment, which reveals the meso-scale heterogeneous features of the front system. In general, there are strong temperature gradients in the north region of the front system but rather weak ones in the south region, the temperature gradient in the middle section over Taiwan Island is complicated because of the underlying surface and effect of topography. The intensity and vertical distribution pattern of the temperature gradient at the same place varies with time. As the front approaches the Island, the frontal temperature gradient is folded by the topographic effect, which makes the temperature gradient increase or decrease. The vertical extension of the temperature gradient also changes, which causes the maximum centers to occur in high levels. As the front moves off the Island, the temperature gradient maxima on the Taiwan Island are limited to rather low levels. So the temperature gradient maxima on the Taiwan Island are closely related to the front system.

All the above indicate that the temperature gradient maxima in the front system are heterogeneous, which leads to different development and evolvement stages for the heavy rain and finally to the heterogeneous precipitation distribution.

### **4.2** Structure of the frontal circulation

An abundant water vapor supply and a strong lift-condensation are two requirements for heavy rain. This section studies the vertical velocity on south, middle and north sections and its evolvement process from 13 to 15 June. At 1800 UTC 13 June, there were two maximum centers of upward velocity on the south section: one at 500 hPa and another at 200 hPa with values of 0.1 m $\mathrm{s}^{-1}$ and 0.2 m $\mathrm{s}^{-1}$ respectively. On the north section, the front is located over the coastal area of the continent (49th latitudinal grid point), the upward movement was clear before the front, the vertical velocity was 0.15 m $\mathrm{s}^{-1}$, and the large value center was at 500 hPa. On the windward slope of Taiwan Island (62th latitudinal grid point), the maximum upward velocity center with a value of 0.15 m $\mathrm{s}^{-1}$ was at 300 hPa. Another center of 0.15 m $\mathrm{s}^{-1}$ preceding the front was on the 350 hPa level.

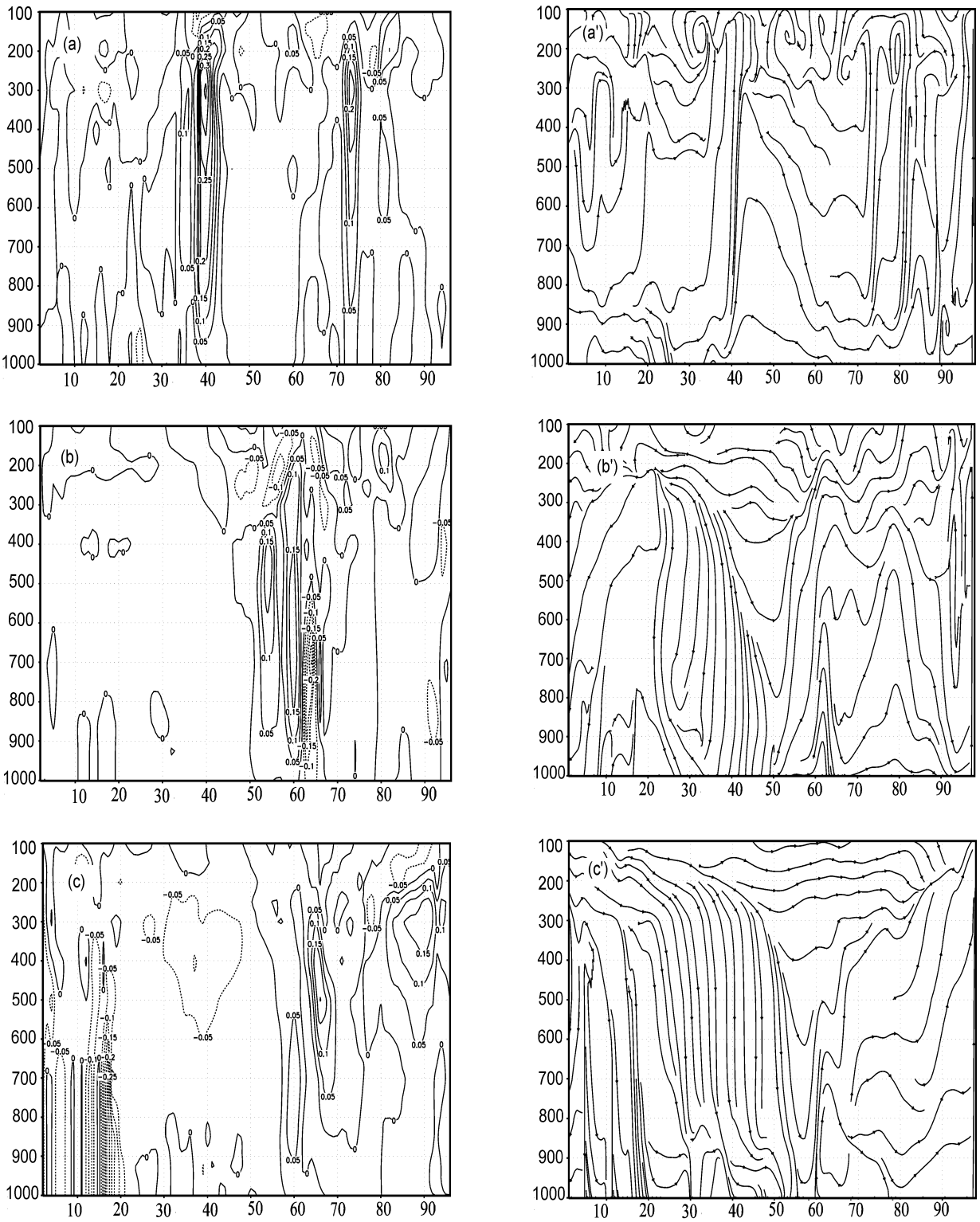


**Fig. 5.** Vertical velocity (a, b, c) (units: m $s^{-1}$) and corresponding streamlines (a′, b′, c′) on latitudinal sections at 0000 UTC 14 June 2001 (a, b and c are south, middle and north sections respectively).

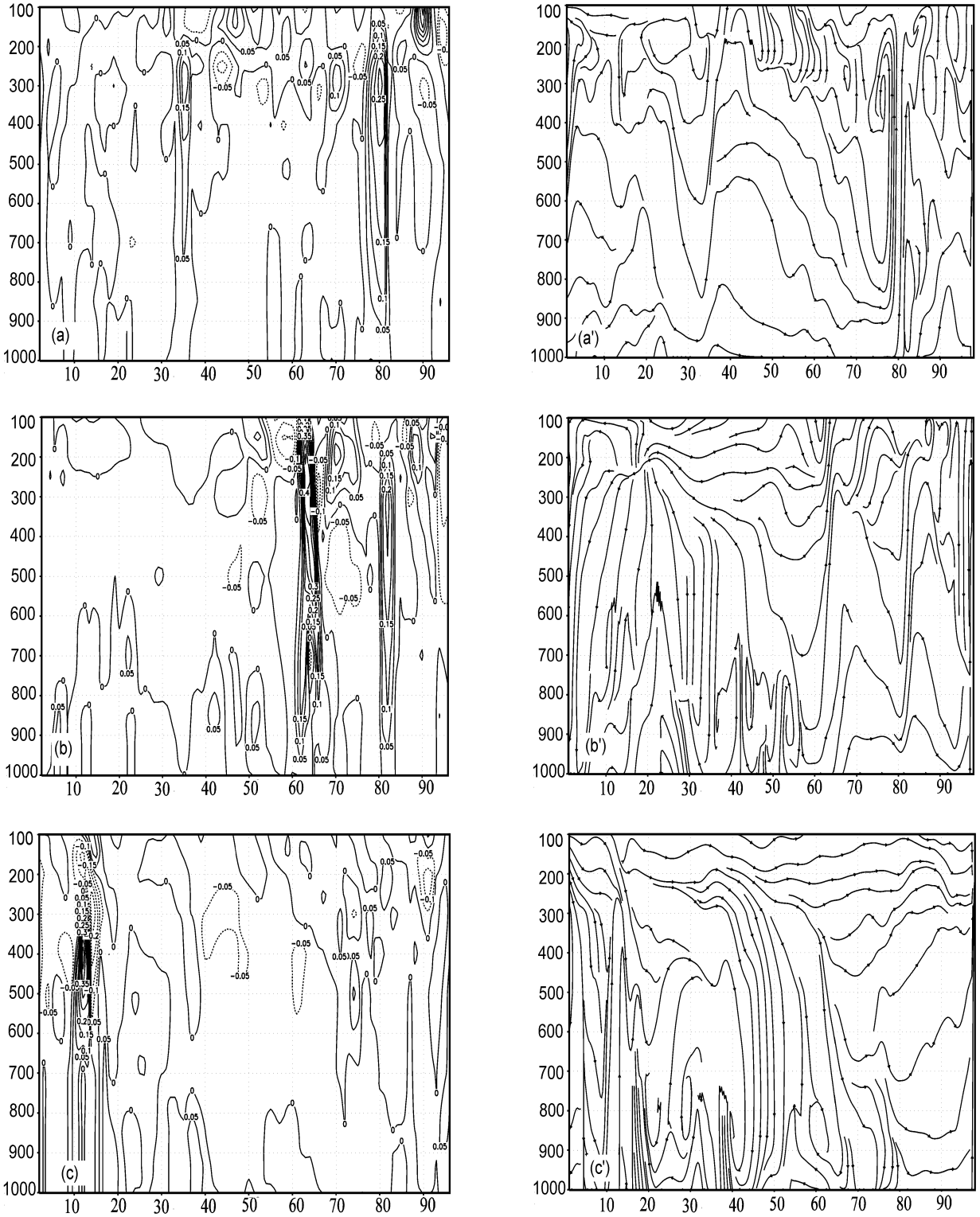


**Fig. 6.** Same as Fig. 5. but at 1200 UTC 14 June 2001.

At 0000 UTC 14 June, the streamline on the south section (Figs. 5a, 5a′) shows that updraft current before the front was very strong and extended vertically to 200 hPa, and the maximum center of 0.3 m s$^{-1}$ was at 300 hPa. The frontal updraft was concordant with the high value area of water vapor, which lifted the low level water vapor to upper levels. The downdraft wind occurred behind the front. On the middle section (Figs. 5b, 5b′), the front was over the Taiwan Strait, and Taiwan Island was in the windward updraft area before the front, where the maximum vertical velocity was 0.15 m s$^{-1}$. To the lee side, downdraft prevailed below 600 hPa; the least value was –0.2 m s$^{-1}$ on the 700 hPa level. The streamline graph shows that there were two opposite vertical circulations related to the front and topography respectively. The north section (Figs. 5c, 5c′) shows the updraft with a maximum value of 0.15 m s$^{-1}$ before the front and the downdraft behind the front.

At 1200 UTC 14 June, the pre-frontal updraft decreased on the south section (Figs. 6a, 6a′), the maximum value was 0.15 m s$^{-1}$, and downdraft appeared in upper levels. The streamline graph shows that the vertical circulation leaned toward the cold area. The middle section shows that the front was over the Taiwan Strait, and the streamline graph shows there was an upper level vertical circulation in the eastern part of Taiwan Island. Furthermore, the updraft branch of the circulation was folded by both frontal and topographical upward current. The vertical velocity over Taiwan Island increased, and the maximum value was 0.4 m s$^{-1}$ on the 200 hPa level. In the low levels, vertical velocity changed less and downdraft decreased on the lee side. On the north section (Figs. 6c, 6c′), the pre-frontal updraft decreased and downdraft dominated most areas.

At 1800 UTC 14 June (figures omitted), the updraft area on the south section moved eastward continuously with a maximum value of 0.15 m s$^{-1}$ on the 400 hPa level. There was a weak downdraft behind the front. On the middle section, the front was over Taiwan Island and upward movement appeared in low levels of the windward slope only; on the middle and upper levels, subsidence prevailed. At that moment, downdraft current behind the front counteracted the upward motion by topographical lifting. The downward movement decreased continuously, and the minimum value was –0.1 m s$^{-1}$ only. On the north section, the upward area moved eastward continuously, its intensity varied less, and the maximum center moved up from 350 hPa to 300 hPa. The streamline graph shows that there was a weak downward current behind the front.

At 0000 UTC 15 June (figures omitted), the pre-frontal updraft was enhanced continuously on the south section, and the maximum value of 0.2 m s$^{-1}$ was on the 350 hPa level. The middle section shows that the front had moved off Taiwan Island, and the pre-front updraft recovered. The streamline graph shows that the low level upward motion on the windward slope recovered as well, while the downdraft prevailed in upper levels. The subsidence current dominated the lee side, which illustrates that topography caused low-level upward motion on the windward slopes. The pre-frontal updraft was enhanced on the north section, the maximum value of 0.35 m s$^{-1}$ was at 350 hPa, and the streamline graph shows that there was subsidence behind the front and that the pre-front upward motion extended to 100 hPa.

Based on the analysis of the distribution and evolvement of vertical velocity on three different sections, we find that the intensity and extending heights of vertical velocity within a frontal system are different everywhere and vary with time as well. The local factors, such as underlying surface, topography and local circulations are all reasons behind the differences. Particularly in Taiwan Island, where protruding topography exists; the upward wind persists on the windward slope, and when it is folded with a front system, the intensity and extent of the updraft increases fast. As the front approaches Taiwan Island, the subsidence behind the front counteracts the topographical lifting; this causes a decrease of upward motion on the windward slope. On the lee side, however, the frontal upward motion can be counteracted by topographical subsidence. In the lower reaches of the lee side, disturbances exist, and these spread leeward and produce intercrossing areas of updraft and downdraft which are shown on streamline graphs as lee waves. The heterogeneous distribution of vertical velocity and the variations of vertical flow caused by the interaction between frontal system and topography are other reasons behind the heterogeneous distribution of heavy rain both in time and in space.

## 5. Front-related upper- and low-level jets and their impact on heavy rain

There is a low-level jet (LLJ) parallel to the front in the northeast-southwest orientation at 925 hPa (Figs. 7a and 7b) which consists of several high wind speed centers distributed in the south, middle, and north sections of the jet band. The average wind speed of these centers is about 18 m s$^{-1}$, and the middle center lies across Taiwan Island.

At 1800 UTC 13 June, a high wind speed center lay in the windward area of Taiwan Island, and the

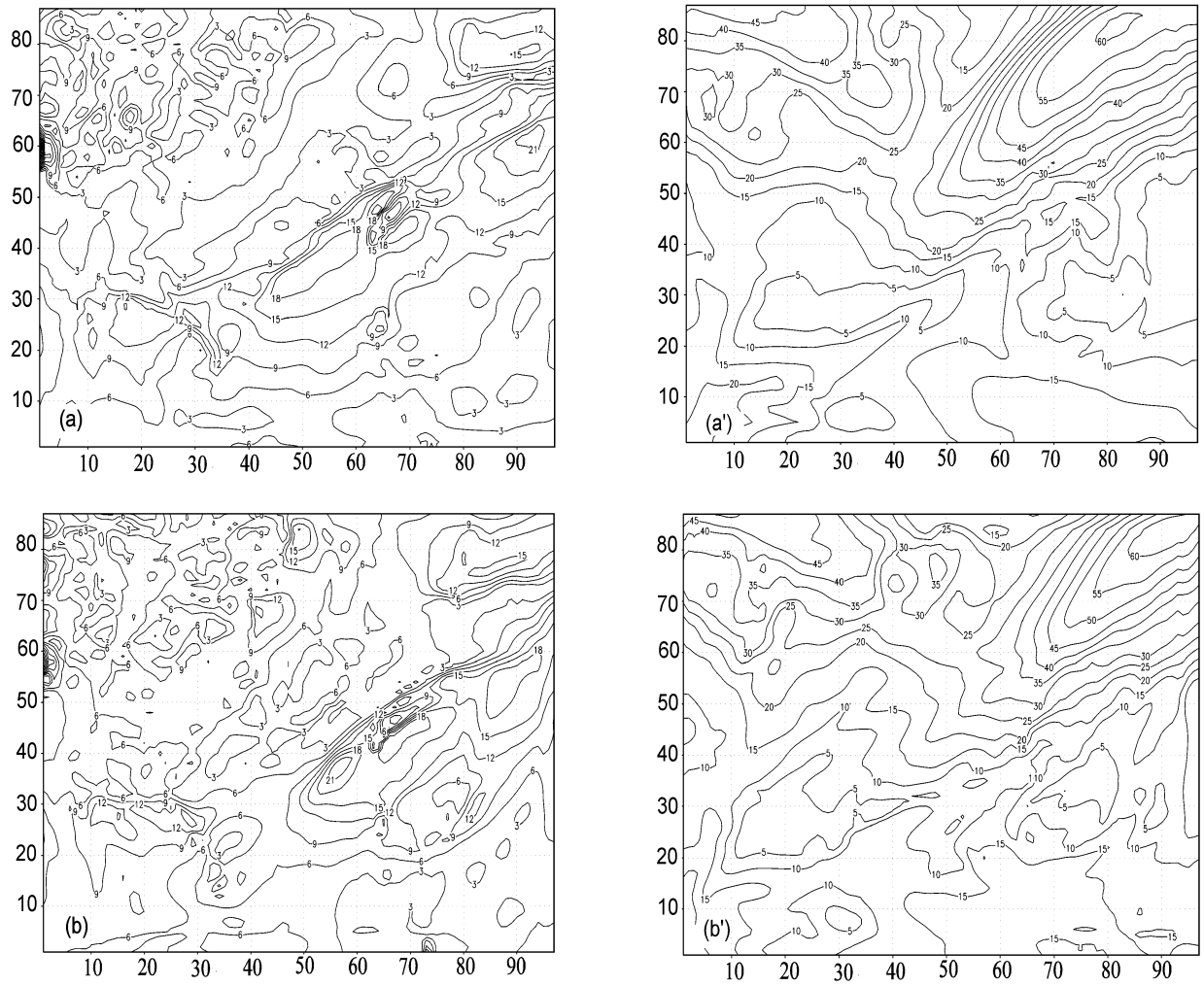


**Fig. 7.** Wind speed at 925 hPa (a, b) and 200 hPa (a′, b′) at 0000 UTC (a, a′) and 1200 UTC (b, b′) of 14 June 2001 (units: m s$^{-1}$).

maximum wind speed was 20 m s$^{-1}$; on the leeside of Taiwan Island, however, the wind speed was only 5 m s$^{-1}$. At 0000 UTC 14 June, the LLJ moved southeastward, with three separated high wind speed centers located in south, middle, and north sections of the LLJ, respectively, which are hereafter referred to as the south, middle, and north centers (Table 2). Because of the effect of topography, the intensity and moving speed of these three centers differed significantly. The wind speed on the windward side and lee side of Taiwan Island were 21 m s$^{-1}$ and 6 m s$^{-1}$ respectively (Fig. 7a). At 0600 UTC 14 June, the LLJ moved southeastward continually and covered the whole Taiwan Island. The wind speed on the windward side increased to 21 m s$^{-1}$ while that on the lee side decreased to 3 m s$^{-1}$, and at the same time, the vertical velocity on the windward side was intensified because more advective kinetic energy was transformed to potential energy. Downstream of lee area, the wind speed increased and formed a high center; the central value was 21 m s$^{-1}$. At 1200 UTC 14 June, the maximum wind speed appeared in the LLJ's south section with a maximum value of 21 m s$^{-1}$, and the wind speed of the other two centers in the middle and north sections of the LLJ were 18 m s$^{-1}$. The wind speed in the windward area of Taiwan Island decreased to 12 m s$^{-1}$ and that in the lee area was 3 m s$^{-1}$ (Fig. 7b). At 1800 UTC 14 June, the LLJ moved away from Taiwan Island. The central value of the north center was 27 m s$^{-1}$ and the other two were 18 m s$^{-1}$. The wind speed difference between the windward and lee areas decreased. At 0000 UTC 15 June, the LLJ moved over the West Pacific Ocean, and the wind speed became uniform along the jet because the effect of the topography of Taiwan Island disappeared. Consequently, the wind speed difference between the windward and lee-

**Table 3.** The intensity and locations of heavy rain centers and the frontal rain band (units: mm).

| Time June 2001 | Centers and central values of precipitation | Location of the frontal rain band |
|---|---|---|
| 0000 UTC 14 June | North center, 4 mm; middle center, 5 mm | southeast coast of China |
| 0600 UTC 14 June | North center, 5 mm; middle center, 9 mm; southern Taiwan Island, 3 mm | Moved southeastward to east Taiwan Strait |
| 1200 UTC 14 June | North center, 6 mm; middle center, 11 mm; South center, 5 mm; Taiwan Island, 9 mm | Move southeastward and close to Taiwan Island |
| 1800 UTC 14 June | North center, 6 mm; middle center (Taiwan Island), 12 mm; North center, 6 mm; | Reached Taiwan Island |
| 0000 UTC 15 June | North center, 6 mm; middle center, 12 mm; South center, 6 mm; Taiwan Island, 10 mm | Moved away from Taiwan Island |

ward areas of Taiwan Island decreased.

The upper-level jet (ULJ) on the 200 hPa level was behind the LLJ (Figs. 7a′ and 7b′), and the maximum wind speed was above 55 m $s^{-1}$. The ULJ also moved southeastward as did the LLJ. It is evident that both the ULJ and LLJ and their interaction were beneficial to the development of heavy rain.

The variation of the LLJ intensity as it passed Taiwan Island reveals the interaction process with the topography. The wind speed in the LLJ's middle center changed significantly because of the topographical resistance. As the front was nearing Taiwan Island, the wind speed in the windward area intensified while that in lee side remained low. The horizontal kinetic energy was transformed into potential energy to increase the vertical velocity, consequently, the horizontal velocity decreased and the vertical velocity increased (Figs. 5 and 6). We find that the location of the high wind speed centers in the LLJ coincide with those of the high temperature gradient centers, which reveals the importance of the optimum cooperation between the dynamic and thermodynamic mechanisms. The optimum cooperation between the ULJ and LLJ is also important in triggering the heavy rain.

## 6. The structure and development of the frontal rain band

Table 3 lists the intensity and locations of the heavy rain centers and the frontal rain band. The rain band also lay in the northeast-southwest orientation as did the LLJ, the high temperature gradient, and the strong wind speed zone. The rain band was heterogeneous and consisted of three heavy rain centers at the north, middle, and south parts of the band. Precipitation at the middle part of the rain band in the windward area was reinforced when the front moved close to Taiwan Island. Precipitation intensity in the windward area weakened as the front moved away from Taiwan Island, which proves again that the precipitation was caused mainly by the front and its interaction with the heterogeneous topography of Taiwan Island.

## 7. Summary and conclusions

A frontal heavy rain procedure that happened over Taiwan Island in June 2001 is studied using the mesoscale model MM5 (V3). The model outputs are analyzed to understand the formation, development, and degradation mechanism of the frontal heavy rain and the interaction process between the frontal circulation and Taiwan Island's topography. The main conclusions are:

(1) The heavy rain that occurs in Taiwan Island is usually caused by the interaction between a southeastward-moving front and the Island's topography.

(2) The temperature gradient, vertical velocities, and horizontal wind speed, etc. within the front system are all distributed heterogeneously in time and space. The heterogeneities become more significant when the frontal system meets the effect of the local topography.

(3) The local factors such as underlying surface properties, prevailing wind, and topographical circulation etc. cause heterogeneity in the vertical velocity in the front system. The thermodynamic heterogeneity of the frontal system is the main reason for the heterogeneous distribution of precipitation and its intensity.

(4) The optimum cooperation of the LLJ and ULJ benefits the development of heavy rain in the frontal rain band.

***Acknowledgments.*** This study was supported by National Natural Science Foundation of China (Grant Nos. 40175012 and 90302015). It was also partly supported by The Innovation Program of Chinese Academy of Sciences (Grant No. ZKCX2-SW-210) and the National Key Basic Research Development Program of MSTC (Grant No. G1999043400).

## REFERENCES


Chen, Y.-L., and J. Li, 1995: Large-scale conditions favorable for the development of heavy precipitation during TAMEX IOP3. *Mon. Wea. Rev.*, **123**, 2978–3002.

Chen, Y.-L., X. A. Chen, S. Chen, and Y.-H. Kuo, 1997: A numerical study of the low-level jet during TAMEX IOP 5. *Mon. Wea. Rev.*, **125**, 2583–2604

Chen, Y.-L., X. A. Chen, and Y.-X. Zhang, 1994: A diagnostic study of the low-level jet during TAMEX IOP -5. *Mon. Wea. Rev.*, **122**, 2257–2284.

Chen, Yi-Leng, and Mei-Yu Cheng, 2000: Characteristics of rainfall distributions and surface wind fields over the Taiwan area during the 1996 and 1997 Meiyu season. *Proc. Conf. on Weather Analysis and Forecasting*, Taiwan University, 89.

Climatology Data Office of Fujian Province, 1987: *Taiwan's Climate*. Edited by editorial board of *Taiwan Chimate*, China Ocean Press, Beijing, 1–5. (in Chinese)

Cui Chunguang, Min Airong, and Hu Bowei, 2002: Dynamic effect of Mesoscale terrain on "98.7" extremely heavy rain in the east of Hubei Province. *Acta Meteorologica Sinica*, **60**(5), 602–612 (in Chinese).

Hao Weifeng, Su Xiaobin, Wang Qinan, and Kou Zheng, 2001: The observational features and the cause analysis of hilly boundary-layer jet. *Acta Meteorologica Sinica*, **59**(1), 120–128. (in Chinese)

Lai Xinzhi, 2002: Numerical simulation study on mesoscale convective system during Meiyu season of Taiwan—Case TAMEX IOP8. Institute of Atmospheric Physics, Center College of Taiwan, 1. (in Chinese)

Li, J., Y.-L. Chen, and W.-C. Lee, 1997: Analysis of a heavy rainfall event during TAMEX. *Mon. Wea. Rev.*, **125**, 1060–1082.

Lin, P. L., H. C. Lai, and Y. F. Sheng, 2000: A numerical study on a shallow front passage over Taiwan IslandIslandduring TAMEX IOP8. *Proc. Conf. on Weather Analysis and Forecasting*, Taiwan University, 264.

Lou Xiaofeng, Hu Zhijin, Shi Yueqin, Wang Pengyun, and Zhou Xiuji, 2003: Numerical simulation of a heavy rainfall case in South China. *Adv. Atmos. Sci.*, **20**(1), 128–138.

Lu Keli, and Zhao Deming, 1997: Effects of both the condensation process of moisture and upper and low-level jets on the cold-front circulation. *Scientia Atmospherica Sinica*, **21**(3), 317–323. (in Chinese)

Song Weiguo, and Chen Tairan, 2001: On the Influence of water vapor on low-level jet in Meiyu season. *Atmospheric Sciences* (Taiwan), **28**(1), 1–13. (in Chinese)

Sun Jian, Zhao Ping, and Zhou Xiuji, 2002: The mesoscale structure of a south China rainstorm and the influence of complex topography. *Acta Meteorologica Sinica*, **60**(3), 333–342. (in Chinese)

Yeh, H.-C., and Y.-L. Chen, 1998: Characteristics of the rainfall distribution over Taiwan IslandIslandduring TAMEX. *J. Appl. Meteor.*, **27**, 1457–1469.

Yue Caijun, Shou Shaowen, Lin Kaiping, and Yao Xiuping, 2003: Diagnosis of the heavy rain near a Meiyu front using the wet $\boldsymbol{Q}$ vector partitioning method. *Adv. Atmos. Sci.*, **20**(1), 37–44.